UNITECH SELECTED PAPERS

International Scientific Conference
UNITECH`2024

MELTING MECHANISM OF CYLINDRICAL MOLYBDENUM NANOWIRE: A MOLECULAR DYNAMICS SIMULATION STUDY

Unal Domekeli[1*], Murat Celtek[2]

[1]*Dept. of Physics, Trakya University, 22030, Edirne – TÜRKİYE*
[2]*Faculty of Education, Trakya University, 22030, Edirne – TÜRKİYE*

** Corresponding author: unaldomekeli@trakya.edu.tr*

Abstract

Nanowires have many unique mechanical, electronic, optical, catalytic and thermodynamic properties, unlike bulk states, due to their high surface/volume atom ratio. Due to these properties, nanowires play an important role in the development of many miniature devices in the field of nanotechnology. The behavior of nanowires under high temperature and pressure should be characterized for the durability of these devices. Therefore, understanding the melting mechanisms of nanowires is very important. In this study, the melting mechanism of cylindrical molybdenum (Mo) nanowire was investigated by molecular dynamics (MD) simulation using long-range Finnis-Sinclair (FS) type potentials. In order to understand the melting mechanism of the nanowire, it was divided into five regions, each with a thickness of $2a_o$, four cylindrical shells and a core. The melting mechanism was characterized by analyzing the thermal, structural and dynamic properties in each region. The results show that the melting of Mo nanowire occurs in two stages. First, a liquid-like shell forms in the outer regions of the nanowire as the temperature increases. The thickness of the liquid-like shell increases with increasing temperature until the shell reaches a critical thickness. Then, the entire nanowire, including the solid-like regions associated with the core, melts homogeneously.

Keywords: Molybdenum nanowire, MD simulations, melting mechanism, FS potentials.

INTRODUCTION

Nanowires (NWs), one of the one-dimensional nanostructures, have unique mechanical, thermal and electronic properties, unlike the bulk form, due to their high surface area to volume ratio [1–3]. These unusual properties have increased the interest in NWs and have provided the opportunity to be used in many different research and application areas. NWs play an important role in the design and fabrication of electro-mechanical devices, especially at the nanoscale [4,5]. Therefore, the deformation mechanisms and thermal stability of NWs should be investigated comprehensively. Many experimental studies have been carried out to determine the thermal, mechanical and electrical properties of NWs [6–8]. Experimentally, the deformation and melting processes of NWs are quite difficult to study at the atomic scale due to many factors such as temperature, orientation, surface and boundary conditions. Due to these factors, NWs may exhibit unpredictable behavior under experimental conditions [9]. To overcome this difficulty, MD simulation technique is a good alternative to experimental methods. MD simulations are quite successful in investigating the deformation and melting processes of NWs at the atomic scale [5,9–13]. Recently, a large number of metallic NWs can be produced by new nano-material manufacturing methods. One of the NWs produced by this manufacturing technique is Mo NW. As it is known, bulk Mo is a metal with high tensile strength, excellent mechanical and electronic properties, and good thermal stability due to its high melting point [14]. There are many MD simulation studies on the mechanical and thermal properties of Mo NWs [14–17]. For example, Peng et al. [15] investigated the deformation mechanism of Mo NWs using MD simulation. They reported that the

doi: www.doi.org/10.70456/LPWG1883

plastic deformation in Mo NWs varies depending on both the lateral size and orientation of the wire. Lin et al. [14] examined the mechanical and thermal stability of ultrathin Mo NWs by performing MD simulation with tight-binding potential. They indicated that the structure of ultrathin Mo NWs differs from the body-centered cubic (bcc) crystal in terms of their mechanical and thermal properties. Although there are many studies on the mechanical properties of Mo NWs, there are very few studies on their melting mechanisms. With this motivation, we comprehensively investigated the melting mechanism of Mo NW using MD simulation in this study.

EXPOSITION

MD simulations for Mo NW and bulk were performed using the parallel code DLPOLY simulation package [18]. As is known, the accuracy of the products obtained from an MD simulation depends significantly on the interatomic interaction potential used in the simulation. Therefore, the long-range FS EAM potential, which can successfully describe the interactions between Mo atoms in MD simulations, was preferred in this study. The total energy of the FS potential, E_{tot}, for a system of N atoms is written by [19,20]:

$$E_{tot} = \frac{1}{2}\sum_i \sum_j V_{ij}(r_{ij}) - A\sum_i \sqrt{\rho_i}, \quad (1)$$

$$V_{ij} = \begin{cases} (r_{ij}-c)^2 (c_o + c_1 r_{ij} + c_2 r_{ij}^2) & (r_{ij} \le c), \\ 0 & (r_{ij} > c), \end{cases} \quad (2)$$

$$\rho_i = \sum_{i \ne j} \phi(r_{ij}), \quad (3)$$

$$\phi_{ij} = \begin{cases} (r_{ij}-d)^2 \dfrac{\beta(r_{ij}-d)^3}{d} & (r_{ij} \le d), \\ 0 & (r_{ij} > d), \end{cases} \quad (4)$$

where r_{ij} is the distance between atoms i and j. $V(r_{ij})$ is the pair potential energy and is the repulsive term of the total energy. ρ_i is the total electronic charge density at the site of atom i, constructed by superposition of the local atomic charge densities. $\Phi(r_{ij})$ is atomic charge density function. A is the embedding energy and forms the attractive term of the total energy expression. β, c_o, c_1 and c_2 are adjustable parameters used in the fitting process. c and d are cutoff parameters. The potential parameters obtained for Mo by Finnis et al. [19] are given in Table 1.

Table. 1. *FS potential parameters for Mo* [19].

parameter	value	parameter	value
A (eV)	1.887117	c_o	43.4475218
c (Å)	3.25	c_1	−31.9332978
d (Å)	4.114825	c_2	6.080424
β	0		

The model cylindrical NW used in MD simulations was obtained by applying a cylindrical wire cutting process of diameter d and height H from bcc crystal as in the diagram shown in Figure. 1.

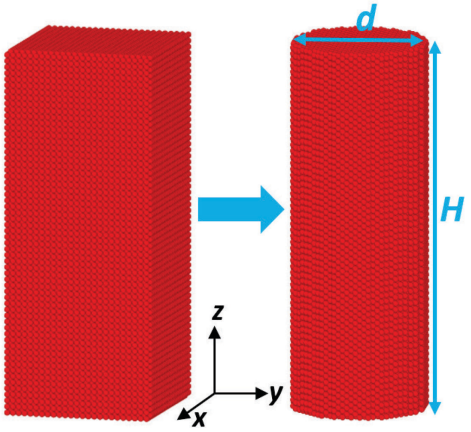

Fig. 1. *Schematic diagram of model Mo NW.*

The diameter (d), height (H) and number of atoms (N) of the model NW are given in Table 2.

Table 2. *The diameter (d), height (H) and number of atoms (N) of Mo NW.*

Symbol	N	d (nm)	H (nm)
NW	46620	7.0	18.9

The NW was simulated under constant volume and constant temperature NVT ensemble with periodic boundary conditions in one dimension, while the bulk system was simulated under constant

temperature and constant pressure NPT ensemble with periodic boundary conditions in three dimensions. The classical equations of motion are integrated using the Leapfrog-Verlet algorithm with a time step of 1fs. The temperature and pressure of the system are controlled by the Nose-Hoover thermostat and the Berendsen borastat, respectively. The stable structure at 0 K was obtained by first annealing the initial configuration at T=300 K using 100000 MD time steps and then cooling it to T=0 K with a cooling rate of 0.05 K/ps. The annealed NW is almost identical to the initial configuration except for the relaxed surface atoms. For NW and bulk, the system was subjected to a heating process consisting of a series of MD simulations with a temperature increase of ΔT=100 K. Around the melting point (T_m), the temperature increment was reduced to ΔT=10 K, taking into account large temperature fluctuations. Simulations were performed at each temperature for 100000 MD time steps. The first 50000 MD time step of the 100000 MD time steps was used to equilibrate the system and the last 50000 MD time steps was used to generate the time averaged features.

In the results section, we first studied the temperature-dependent variation of caloric curves such as potential energy and heat capacity to observe the transition from solid phase to liquid phase for Mo NW during the melting process. For this purpose, the potential energy and heat capacity as a function of temperature for Mo NW and bulk system are shown in Figure 2. At low temperatures, the potential energy of NW and bulk increases linearly with temperature. However, a sudden jump occurs in the energy curve at the temperature at which the transition from solid to liquid phase occurs. The temperature at which the jump in potential energy occurs is defined as the T_m of the system. At temperatures above the T_m, the caloric curve continues its linear behavior as in the low temperature region. Also, the potential energy of NW is higher than that of bulk. This can be explained by the fact that NW has a large surface energy due to its high surface area-to-volume ratio. The slope of the heat capacity curve given in Figure 2 increases significantly at the temperature where the sudden jump in potential energy occurs. This behavior observed in the heat capacity indicates that the system has undergone a first-order phase transition. At low temperature (room temperature), the value of the heat capacity for both the NW and bulk systems goes to the Dulong-Petit value for harmonic solids ($C_p \approx 25$ $Jmol^{-1}K^{-1}$). The melting temperatures predicted from the characteristic behavior of both potential energy and heat capacity are 2970 K and 3490 K for the Mo NW and bulk system, respectively. NW has lower melting point than the bulk system due to its higher surface energy.

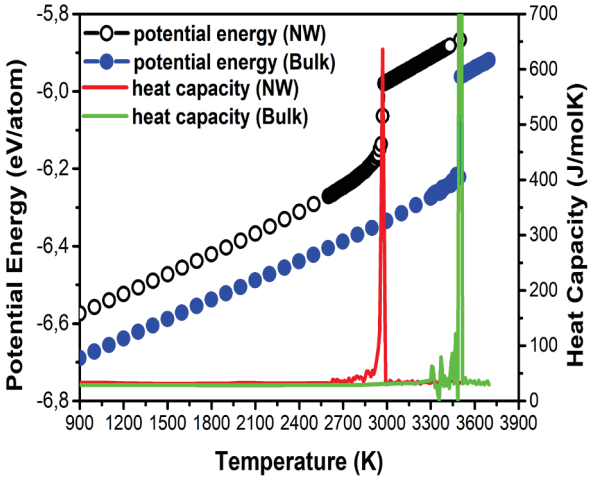

Fig. 2. *Temperature dependent variation of the potential energy and heat capacity for Mo NW and bulk system.*

Pair distribution function (PDF) describes the probability of finding another particle at a distance r from a reference atom. The PDF depends greatly on the type of matter, thus it varies greatly for solids, amorphous, liquids and gases. Therefore, The PDF is the most important structural function that is frequently used to analyze structural properties, whether the system is crystalline or non-crystalline. The expression of the PDF, $g(r)$, is as follows [21]:

$$g(r) = \frac{\Omega}{N^2}\left\langle \sum_{i}^{N}\sum_{i\neq j}^{N}\delta(r - r_{ij}) \right\rangle \quad (5)$$

where N and Ω represent the number of atoms, and volume of the simulations cell, respectively. Figure 3 shows the PDFs of Mo NW at different temperatures during heating-process. The PDF exhibits the characteristic behavior of an ideal bcc crystal structure at 900 K. As the temperature increases, the peak amplitudes of the PDF decrease and the peak widths increase. At T_m=2970 K, it is understood from the PDF behavior that there is atomic structural order representing both solid and liquid phases in the NW. As is known, during a phase transition, the structural behavior of a system is a mixture of solid and liquid phases. At 2980 K, above the T_m, the PDF of the NW exhibits completely liquid phase characteristics. These structural results support the accuracy of the T_m predicted from thermal properties for NW.

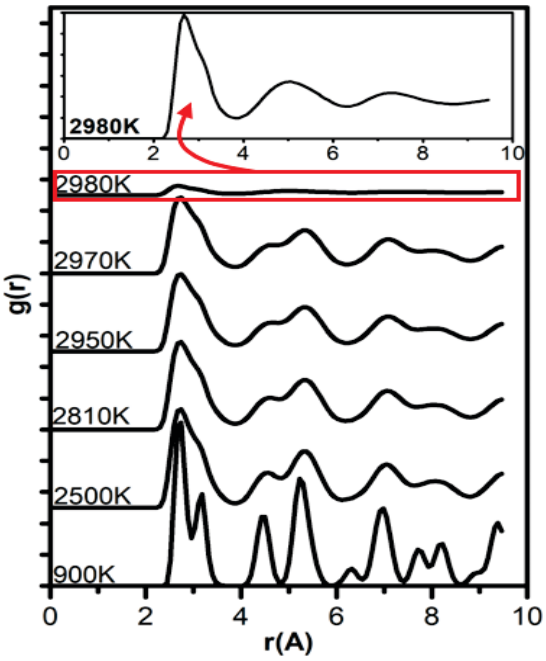

Fig. 3. *PDFs of Mo NW at different temperatures during the heating-process.*

In order to explain the melting mechanism of NW, the cylindrical wire was divided into five regions, each with a thickness of $2a_o$ (a_o=3.15Å [22] for Mo), consisting of four cylindrical shells and core. These cylindrical shells were labeled 1. shell, 2. shell, 3. shell, 4. shell and core, respectively, from outermost to innermost (see Figure 4). Thanks to this labeling, the atomic motion in each shell during the heating process can be easily monitored and in-depth information about the melting mechanism of the NW can be obtained. Snapshots of the atomic positions projected onto the xy plane for the NW at different temperatures are shown in Figure 4.

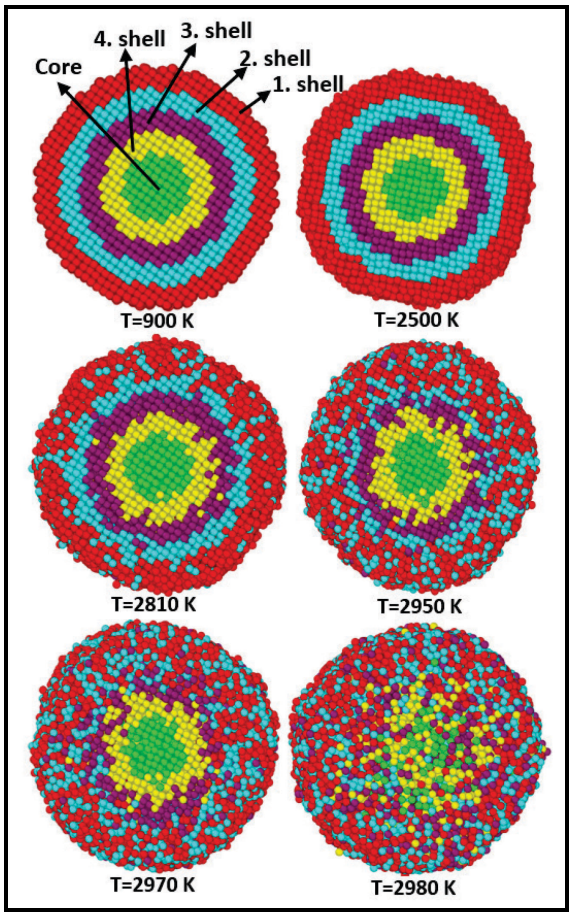

Fig. 4. *Snapshots of the projected atomic positions of NW during the heating process.*

As seen in Figure 4, at 900 K, the atoms in each shell and core maintain their bcc crystal lattice positions. When the temperature is 2500K, the metallic bonds between the atoms in the first shell are broken and the atoms move away from the lattice points, forming a liquid layer in the outermost region of the NW. However, the other shell and core atoms maintain their current bcc crystal structure. At 2810 K, the

liquid layer formed in the outermost shell spreads into the NW and the 2. shell becomes completely liquid. However, the other regions still maintain their crystalline state. It is seen from the atomic configuration that the 3. shell starts to melt at 2950 K. At T_m=2970 K, the 1., 2. and 3. shells are completely in the liquid phase, while the 4. shell and the core largely retain their crystalline structure. At 2980 K, above the melting point, the atomic configuration shows that the 4. shell and core regions are melted and the NW is completely in the liquid phase. The best way to determine the atomic mobility in the NW during the melting process is to calculate the self-diffusion coefficient from the dynamic properties. The self-diffusion coefficient, D, is calculated by using the Einstein equation:

$$D = \lim_{t\to\infty} \frac{MSD}{6t} \qquad (6)$$

where t is the diffusion time, MSD of the atom in the MD simulations can be described as [20]:

$$MSD = \frac{1}{N}\sum_{i=1}^{N} \left| r_i(t+t_o) - r_i(t_o) \right|^2 \qquad (7)$$

where $r_i\,(t_o)$ is the position vector of the ith atom for the system in its initial configuration and $r_i\,(t)$ is the position vector of ith atom at time t.

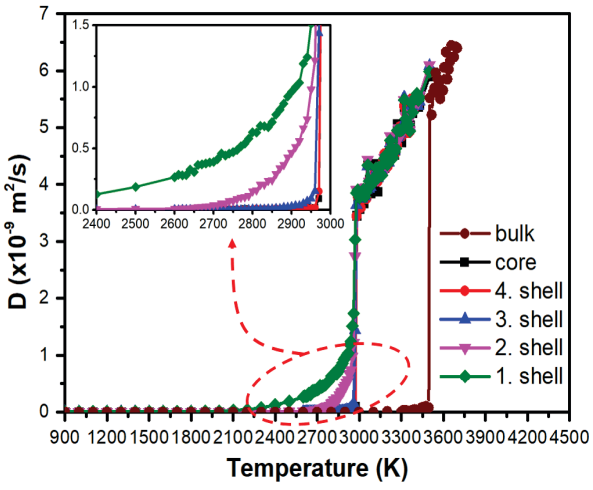

Fig. 5. *Variation of self-diffusion coefficients as a function of temperature for Mo NW and bulk.*

In Figure 5, the self-diffusion coefficients obtained from the MD simulation for each region in the NW and the bulk system are shown as a function of temperature. In the low temperature region (i.e. 300 K-2400 K) the self-diffusion coefficient is around zero as in the crystalline phase. Between about 2400 K and the melting point, there is an increase in the diffusion coefficient as in the liquid phase in the 1., 2. and 3. shells, respectively (see inset of Figure 5). This increase is a clear indication that these shells are in the liquid phase. The self-diffusion coefficients of the 4. shell and core increase abruptly at the melting point, similar to those of the bulk system. These results support the behavior of the snapshots of atomic positions given in Figure 4 at different temperatures. For the NW, both the snapshots of atomic positions and the temperature-dependent behavior of the self-diffusion coefficients indicate that the melting of the NW occurs in two stages: first pre-melting and then homogeneous melting as in the bulk system.

CONCLUSION

In this study, the melting mechanism of cylindrical Mo nanowire was investigated by MD simulation with long-range FS type potentials. The core/shell based sampling modeled in the MD simulation shows that the melting starts from the surface of the NW. A liquid-like shell forms in the outer regions of the NW. This liquid shell progresses towards the interior of the NW with increasing temperature until it reaches a critical thickness. This critical thickness is approximately $6a_o$, corresponding to the first three shell thicknesses of the studied NW. Then the remaining part of the wire melts homogeneously as in the bulk system and thus the NW is completely melted. Also, since NW has a high surface area to volume ratio, its potential energy at the same temperature (e.g. 900 K) is higher than that of the bulk. Since NW undergoes surface melting, unlike the bulk, it has a lower melting temperature than the bulk.

Acknowledgments: We would like to thank Trakya University Rectorate for giving

permission and contributing to present this study as a paper.

REFERENCE

[1] H.S. Park, J.A. Zimmerman, Modeling inelasticity and failure in gold nanowires, Phys. Rev. B 72 (2005) 054106.

[2] S. Suresh, J. Li, Deformation of the ultra-strong, Nature 456 (2008) 716–717.

[3] Y. Gao, Y. Sun, X. Yang, Q. Sun, J. Zhao, Investigation on the mechanical behaviour of faceted Ag nanowires, Mol. Simul. 42 (2016) 220–228.

[4] Y. Gan, J.K. Chen, Molecular dynamics study of size, temperature and rate dependent thermomechanical properties of copper nanofilms, Mech. Res. Commun. 36 (2009) 838–844.

[5] Y. Jing, Q. Meng, W. Zhao, Molecular dynamics simulations of the tensile and melting behaviours of silicon nanowires, Phys. E Low-Dimensional Syst. Nanostructures 41 (2009) 685–689.

[6] K. Lee, Z. Wu, Z. Chen, F. Ren, S.J. Pearton, A.G. Rinzler, Single Wall Carbon Nanotubes for p-Type Ohmic Contacts to GaN Light-Emitting Diodes, Nano Lett. 4 (2004) 911–914.

[7] A. Du Pasquier, H.E. Unalan, A. Kanwal, S. Miller, M. Chhowalla, Conducting and transparent single-wall carbon nanotube electrodes for polymer-fullerene solar cells, Appl. Phys. Lett. 87 (2005) 203511.

[8] J. Li, L. Hu, L. Wang, Y. Zhou, G. Grüner, T.J. Marks, Organic Light-Emitting Diodes Having Carbon Nanotube Anodes, Nano Lett. 6 (2006) 2472–2477.

[9] S. Kazanç, C. Aksu Canbay, Molecular dynamic simulation of uniaxial tension deformation applied to α-Fe nanowire, Turkish J. Eng. 6 (2022) 190–198.

[10] J. Wang, X. Chen, G. Wang, B. Wang, W. Lu, J. Zhao, Melting behavior in ultrathin metallic nanowires, Phys. Rev. B 66 (2002) 085408.

[11] D.W. Shi, L.M. He, L.G. Kong, H. Lin, L. Hong, Superheating of Ag nanowires studied by molecular dynamics simulations, Model. Simul. Mater. Sci. Eng. 16 (2008) 025009.

[12] W.X. Zhang, C. He, Melting of Cu Nanowires: A Study Using Molecular Dynamics Simulation, J. Phys. Chem. C 114 (2010) 8717–8720.

[13] Sedat Sengul, Unal Domekeli, M. Celtek, Melting Behavior of Pb Nanowires: Molecular Dynamics Simulations, , International Scientific Conference UNITECH 2020, Gabrovo, 2020: p. 381.

[14] K.-H. Lin, B.-Y. Liao, S.-P. Ju, J.-S. Lin, J.-Y. Hsieh, Mechanical properties and thermal stability of ultrathin molybdenum nanowires, RSC Adv. 5 (2015) 31231–31237.

[15] P. Wang, W. Chou, A. Nie, Y. Huang, H. Yao, H. Wang, Molecular dynamics simulation on deformation mechanisms in body-centered-cubic molybdenum nanowires, J. Appl. Phys. 110 (2011) 093521.

[16] X. Li, W. Hu, S. Xiao, W.-Q. Huang, Stress-induced phase transformation and strain rate effect in polycrystalline Mo nanowires, Phys. E Low-Dimensional Syst. Nanostructures 43 (2011) 1131.

[17] J. Wang, W. Hu, X. Li, S. Xiao, H. Deng, Strain-driven phase transition of molybdenum nanowire under uniaxial tensile strain, Comput. Mater. Sci. 50 (2010) 373–377.

[18] W. Smith, T.R. Forester, DL_POLY_2.0: A general-purpose parallel molecular dynamics simulation package, J. Mol. Graph. 14 (1996) 136–141.

[19] M.W. Finnis, J.E. Sinclair, A simple empirical N -body potential for transition metals, Philos. Mag. A 50 (1984) 45–55.

[20] S. Sengul, M. Celtek, U. Domekeli, The Structural Properties Of Liquid Molybdenum Under High Pressure: Molecular Dynamics Simulations Study, International Scientific Conference UNITECH 2021, Gabrova, 2021: pp. II–313.

[21] U. Domekeli, A molecular dynamic study of the effects of high pressure on the structure formation of liquid metallic $Ti_{62}Cu_{38}$ alloy during rapid solidification, Comput. Mater. Sci. 187 (2021) 110089.

[22] C. Kittel, Introduction to the physics of the solid state, University, John Wiley & Sons, Inc, 1986.